Three-Dimensional Ultrasonic Vision for Robotic Applications

ANTHONY S. ACAMPORA, FELLOW, IEEE, AND JACK H. WINTERS, SENIOR MEMBER, IEEE

Abstract—**We consider a vision system that uses the echo of a transmitted ultrasonic pulse as the basis for identifying objects. With this system, the return of a single pulse from an object generates a three-dimensional acoustical characteristic signature across the aperture of a receiving antenna which can be directly used for object identification. Thus, there is no need to reproduce an accurate visual representation in order to recognize which of a class of objects is present. Since the signal bandwidth is narrow relative to that of an optical imaging system, faster execution should be possible. Finally, the need to remove clutter which may arise in a conventional imaging system, caused by the compression of three dimensions into two, is totally avoided.**

However, unlike an optical system, the extent of an object of interest may not be orders-of-magnitude larger than the "beamwidth" of the receiving aperture. We calculate a fundamental limit (in the Shannon sense) on the number of objects that may be distinguished by an ultrasonic system and show that, for modest signal-to-noise ratios and an object space comparable to the beamwidth, an enormous number of different objects may still, in principle, be resolved. Based on these results and on the calculation of signatures of some common geometric shapes, we conclude that the approach offers promise as a complement to or replacement for a conventional optical system, and identify some areas where additional work is needed to realize the full potential of ultrasonic vision.

Index Terms—**antennas, 3-D acoustic signature, robotics, ultrasonic pulses, ultrasonic vision.**

I. Introduction

THE widespread interest in factory automation and robotics has spurred increasing research into the field of machine vision and pattern recognition [1]. Most of this research centers on vision systems using natural or structured light to illuminate objects of interest and use a visual, camera-produced two-dimensional image of the scene as the basis from which recognizable patterns may subsequently be extracted. These approaches encounter two distinct difficulties. First, the scene provided by the front-end camera supplies a vast amount of data, most of which are irrelevant to the robotic task at hand (e.g., the title and illustration appearing on the jacket of a book are irrelevant to the task "find and move the book"). Extraction of that limited amount of information actually needed for task oriented decision making is computationally intensive and time consuming. Second, the camera produces a two-dimensional representation of a three-dimensional world, thereby producing a sea of background clutter which may obscure identification of a near-in object of interest (e.g., pictures or photographs hanging on a wall are indistinguishable from an IC package placed on a bench in front of the wall). Furthermore, the compression of three dimensions into two may obscure the true nature of objects (e.g., spheres appear like circular plates). In short, a vision system that presents data in a format suitable for human comprehension may be less suited for comprehension by a task-oriented machine.

Consequently, to complement the aforementioned computer vision approaches and research directions, we consider a vision system that uses the echo of a transmitted ultrasonic pulse as the basis from which key information may be extracted. The idea of using a time-pulsed sensor to facilitate machine vision is not new [2]–[7]. However, these earlier approaches focus on the generation of surface maps using either a single transducer [2] or a set of transducers [3]–[5] mechanically swept across the field-of-view to slowly produce a three-dimensional surface map of the environment or an array of transducers [6], [7] to quickly generate surface maps. Again, such a map might be useful for human comprehension (for example, medical imaging), but perhaps, be less suitable for a machine. By contrast, the approach that we take seeks the direct identification of objects by virtue of their unique ultrasonic signatures.

In an attempt to simplify and quickly extract key information needed for decision making, we consider a system that receives the echo of a short ultrasonic pulse via a compact, nonswept, narrow-beam ultrasonic antenna having a wide field-of-view. With this system, the return from a single pulse generates a three-dimensional acoustical characteristic signature of each object within the field-of-view. We propose using the signatures of objects contained in some object set of interest as the basis for identifying which object was present and for distinguishing among all possible objects in the set.[1] This approach completely avoids the need to reconstruct a visual representation of the three-dimensional scene but, instead, attempts to directly obtain key features needed to provide rapid identification and distinguishability by homing in on the underlying communication aspect of the problem. In

Manuscript received September 26, 1986; revised November 17, 1987. Recommended for acceptance by W. Eric Grimson.

The authors are with AT&T Bell Laboratories, Holmdel, NJ 07733. A. S. Acampora is on leave at Columbia University, New York, NY 10027.

IEEE Log Number 8825726.

[1]The approach of identifying objects using the acoustic signature has been studied previously for illumination of an object by a continuous (CW) acoustic signal rather than a pulsed signal (see, e.g., [8]).

0162-8828/89/0300-0291$01.00

this context, the problem may be posed as follows. Given one of N possible three-dimensional objects, which one is most likely to have produced this return? As we show, the ability to distinguish among objects is ultimately limited by the signal energy-to-noise density ratio (E/N_o) and certain physical parameters of the imaging system.

A fundamental limitation on the ability of such an imaging system to distinguish among objects is the relationship between the physical extent of the object, in degrees, and the beamwidth of the ultrasonic antenna. Each point-of-reflection on the object's surface produces a diffraction pattern in the focal plane of the antenna whose width varies inversely with the size of the receiving aperture (a wide field-of-view is obtained from a narrow-beam antenna by placing the receiving sensors along a large arc in the focal plane). This smearing of points, which is readily explained via Fourier optics as arising from the suppression of high spatial frequencies, causes a loss of distinguishability as the object size becomes comparable to or smaller than the beamwidth. Fortunately, this loss of distinguishability can be partially offset by using a sufficiently broadband pulse to allow points closely spaced in azimuth and elevation to be distinguished by differences in radial distance from the antenna. In this regard, we parenthetically note that ultrasonic pulses are far superior to microwave or optical pulses because the ultrasonic speed of propagation is five orders of magnitude smaller.

We confine our attention to the distinguishability of three-dimensional signatures (azimuth, elevation, and radial) and explore the relationships between distinguishability, physical parameters, bandwidth, and E/N_o. We postpone for later work the issue of signature variability with object orientation; although related, this issue is more appropriately treated as one of object classification rather than one of object distinguishability.

In Section II, we present a model of the ultrasonic imaging system and define the basic nomenclature. Section III is devoted to understanding the fundamental limitations of the system, and we present an upper bound, in the Shannon sense, on the number of signatures that can possibly be distinguished. Typical results are as follows. Consider all objects located within a volume half as large as the antenna's main lobe in azimuth and elevation and half the spatial extent of the transmitted pulse in depth. At an E/N_o of 20 dB, no more than 94 000 objects may be distinguished; under the same conditions, but with the extent of objects confined to the entire main lobe in azimuth and elevation, the fundamental bound on the number of objects that may be distinguished grows to more than 5×10^{11}. Thus, the system may distinguish among many objects, each smaller than the beamwidth. We also derive an upper bound on the number of objects that may be distinguished subject to some acceptable misidentification criterion. In Section IV, we consider the distinguishability of objects possessing some common geometrical shapes (spheres, cubes, etc.). We first derive a formula for the images of arbitrary objects in the time domain and, using this formula, examine the image of common shapes. Results show that the signal received from objects is mainly from surfaces that are at small angles relative to the wavefront. For example, when the distance to the object is ten times the antenna diameter, the signal power received from surfaces at a 5° angle are 20 dB lower than from surfaces at a 0° angle. We also consider the metric distance between the image of two spheres of various sizes and show that the difference in the shape of the image is an order of magnitude less than the difference in the magnitude of the image. Thus, we must be able to distinguish most objects based on the return from a small portion of the object.

II. System Model

The vision system that we wish to consider is shown in Fig. 1 which, for simplicity, is drawn in two dimensions only (azimuth or elevation and range).[2] An object is illuminated from the right by the spherical wave produced by an ultrasonic point source. The characteristic dimensions of the object are large compared to the ultrasonic wavelength, and the acoustic impedance of the object is much larger than that of air, so that the object appears like a perfect mirror to the ultrasonic illumination. Along a spherical contour located close to the object with the center at the middle of a thin lens, the reflection of the object may be found by ray tracing, that is, along the object sphere, the amplitude and phase of the reflection may be found by tracing each incident ray as it is reflected from the object. For each incident ray, the object's surface normal is found at the point where the ray is intercepted by the object, and the direction of the reflected ray is found by setting the angle of reflection equal to the angle of incidence. The reflected scalar field along the object sphere presents an input to the vision system which is then transformed, in accordance with the principles of Fourier optics, into an image formed along a second spherical contour (the image sphere). In practice, the thin lens would be replaced by an array of small receptors; for now, we assume the existence of many small receivers located along the image sphere which present a continuum of the image to the vision processor.

In the remainder of this section, we briefly review the principles of Fourier optics as they apply to this system in order to establish and clarify the mathematical nomenclature and to pinpoint the approximations made. We also extend these results, which are derived for monochromatic illumination, to treat the case of pulsed illumination.

Assume, to start, that the point source emits a monochromatic wave at frequency ω, and that the reflection of the object cast along the object sphere is $\overline{H}(\alpha, \omega)$ where the overbar denotes a complex valued function. From Green's theorem, the field reflected back to the plane of

[2]To simplify the analysis in Sections II and IV, we consider only two dimensions since the extension of the formulas to three dimensions is trivial.

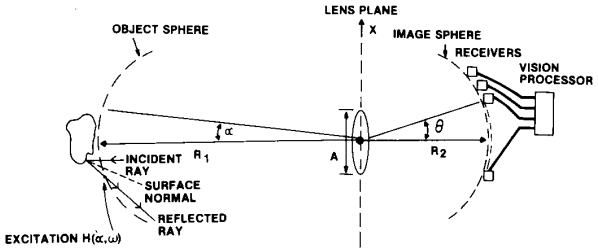

Fig. 1. Ultrasonic vision system.

the lens, $\bar{F}(x, \omega)$, can be represented as

$$\bar{F}(x, \omega) = C(R_1) \int \bar{H}(\alpha, \omega) \cdot \exp\left(jk\sqrt{R_1^2 + x^2 - 2R_1 x \sin\alpha}\right) d\alpha \quad (1)$$

where $C(R_1)$ is a constant depending only on R_1 and $k = \omega/c$ is the wavenumber, with c the speed of propagation.

Suppose $R_1 >> x$. Then,

$$\sqrt{R_1^2 + x^2 - 2R_1 x \sin\alpha} = R_1\sqrt{1 + \frac{x^2}{R_1^2} - \frac{2x}{R_1}\sin\alpha} \doteq R_1\left[1 + \frac{x^2}{2R_1^2} - \frac{x}{R_1}\sin\alpha\right] \quad (2)$$

and

$$\bar{F}(x, \omega) = C(R_1)\, e^{jkR_1} \int \bar{H}(\alpha, \omega) \cdot \exp\left[-jk\left(x\sin\alpha - \frac{x^2}{2R_1}\right)\right] d\alpha. \quad (3)$$

For our purposes, the constant $C(R_1)\, e^{jkR_1}$ is irrelevant and will henceforth be assumed to be of value unity. Assuming α to be a small angle, we obtain the desired result

$$\bar{F}(x, \omega) = e^{jkx^2/2R_1} \int \bar{H}(\alpha, \omega)\, e^{-jkx\alpha}\, d\alpha, \quad (4)$$

i.e., except for the phase factor $e^{jkx^2/2R_1}$, the field reflected at the lens plane is the Fourier transform of the excitation.

Projection through the lens produces an addition quadratic phase shift and also limits the field to that which exists along the aperture of the lens A

$$\bar{G}(x, \omega) = \begin{cases} \bar{F}(x, \omega)\, e^{-jkx^2/2f}, & -\frac{A}{2} \le x \le \frac{A}{2} \\ 0, & \text{otherwise} \end{cases} \quad (5)$$

where f is a characteristic of the lens called the focal length. Again applying Green's theorem to this field appearing just to the right of the lens, we find that over the image sphere

$$\bar{S}(\theta, \omega) = \int_{-A/2}^{A/2} \bar{G}(x, \omega) \exp\left[jk(x^2/2R_2 - x\theta)\right] dx \quad (6)$$

where the same approximations were made as before ($R_2 >> x$, θ small). Substituting (4) and (5) into (6), we obtain

$$\bar{S}(\theta, \omega) = \int_{-A/2}^{A/2} \exp\left[jk(x^2/2R_1 + x^2/2R_2 - x^2/2f)\right] \cdot e^{-jkx\theta} \int \bar{H}(\alpha, \omega)\, e^{-jkx\alpha} d\alpha\, dx. \quad (7)$$

Interchanging the order of integration and applying the lens equation

$$\frac{1}{R_1} + \frac{1}{R_2} = \frac{1}{f} \quad (8)$$

we obtain the principal result

$$\bar{S}(\theta, \omega) = A \int \bar{H}(\alpha, \omega) \frac{\sin\left[k(\theta + \alpha)A/2\right]}{\left[k(\theta + \alpha)A/2\right]} d\alpha. \quad (9)$$

Inspection of (9) reveals that the signal available for detection on the image sphere $\bar{S}(\theta, \omega)$ is of the form of a convolution of the excitation $\bar{H}(\theta, \omega)$ with the pupil function $\sin k\theta/k\theta$. Alternatively, we may view $\bar{S}(\theta, \omega)$ as the response of a spatially band-limited filter to the excitation $\bar{H}(\theta, \omega)$. This filtering, which is the result of the finite lens aperture, distorts and prevents the image from being an exact replica of the excitation; the loss of high spatial frequencies arising from the filter creates a limit on the distinguishability of objects to be recognized by the vision system.

To conclude this section, we derive the response of the system to a pulsed excitation $p(t)$ modulated onto a carrier ω_o. We start with a representation for $\bar{S}(\theta, \omega)$ from which irrelevant factors pertaining to magnification are suppressed, but which preserves all of the salient system features. In this manner, from (9), we define

$$\bar{S}(\theta, \omega) = \int \bar{H}(\alpha, \omega) \frac{\sin\beta(\theta + \alpha)}{\beta(\theta + \alpha)} d\alpha \quad (10)$$

where $\beta\ (= kA/2)$ varies linearly with ω. Referring to Fig. 1 and recalling the principle of ray tracing, we note that the excitation $\bar{H}(\alpha, \omega)$ has amplitude which is independent of the frequency ω and has phase which varies linearly with ω (delay only). Let the delay at angle α be represented by $\tau(\alpha)$. Then,

$$\bar{H}(\alpha, \omega) = H(\alpha)\, e^{-j\omega\tau(\alpha)}. \quad (11)$$

Assume now that, rather than being monochromatic, the point source illumination is of the form $p(t)\, e^{j\omega_o t}$, having Fourier transform $P(\omega - \omega_o)$ where $P(\omega) \Leftrightarrow p(t)$. Since the vision system is linear, superposition applies, and we may view the temporal response $\bar{S}(\theta, t)$ as the linear superposition of sinusoids weighted in accordance with $P(\omega - \omega_o)$. The result from (10) and (11) is

$$\bar{S}(\theta, t) = \iint H(\alpha)\, e^{-j\omega\tau(\alpha)} P(\omega - \omega_o) \cdot \frac{\sin\beta(\theta + \alpha)}{\beta(\theta + \alpha)} e^{j\omega t} d\alpha\, d\omega/2\pi. \quad (12)$$

We assume that the bandwidth of $p(t)$ is small compared to the carrier frequency ω_o (narrow-band assumption) to justify neglecting dispersion caused by the lens pupil function $[\sin \beta(\theta + \alpha)/\beta(\theta + \alpha)]$. Let $\beta_o = \beta(\omega_o)$. Then, reversing the order of integration in (12), we obtain

$$\bar{S}(\theta, t) = e^{j\omega_o t} \int H(\alpha)\, e^{-j\omega_o \tau(\alpha)} p[t - \tau(\alpha)] \cdot \frac{\sin \beta_o(\theta + \alpha)}{\beta_o(\theta + \alpha)}\, d\alpha. \tag{13}$$

As the final exercise, let us consider the baseband representation of the response $\bar{S}(\theta, t)$. Let

$$\bar{H}(\alpha) = H(\alpha)\, e^{-j\omega_o \tau(\alpha)}. \tag{14}$$

We thus obtain our final result

$$\bar{S}(\theta, t) = \int \bar{H}(\alpha) p[t - \tau(\alpha)] \frac{\sin \beta_o(\theta + \alpha)}{\beta_o(\theta + \alpha)}\, d\alpha. \tag{15}$$

Thus, the baseband response appearing along the image sphere of Fig. 1 may be expressed as a sum of delayed versions of the illuminating baseband pulse $p(t)$ weighted by the reflected excitation $\bar{H}(\alpha)$ and filtered by the finite aperture of the lens. The delayed versions of the pulse arise from the depth of the illuminated object. Thus $\bar{S}(\theta, t)$ can alternatively be represented in terms of some spatially and temporally varying excitation $\bar{I}(\alpha, t)$ as

$$\bar{S}(\theta, t) = \int \left[\int \bar{I}(\alpha, \tau)\, p(t - \tau)\, d\tau \right] \cdot \frac{\sin \beta_o(\theta + \alpha)}{\beta_o(\theta + \alpha)}\, d\alpha. \tag{16}$$

From ray tracing, the response caused by illuminating any object with a point source emitting a pulse of energy at the carrier frequency, ω_o may be obtained from (15) or (16).

III. Fundamental Limits

We now consider the fundamental limits of the system described in Section II by analyzing an upper bound, in the Shannon sense, on the number of object signatures that can be distinguished.

Consider a volume in space that defines the extent of objects we wish to distinguish among. Let the location of a point in space relative to the lens be given by its radius r and its directional coordinates α and ϕ. The volume of interest is bounded by angles α_1 and α_2, ϕ_1 and ϕ_2, and radii r_1 and r_2, with $\Delta\alpha = |\alpha_1 - \alpha_2|$, $\Delta\phi = |\phi_1 - \phi_2|$, and $\Delta r = |r_1 - r_2|$. The volume is illuminated by a unit energy pulse $p(t)$ with rectangular signal spectrum of bandwidth $4\pi W$ centered at ω_o. The reflection of this pulse is received through a lens (or by an antenna) of rectangular aperture A_α, A_ϕ. The parameters of interest are 1) B_α, the ratio of $\Delta\alpha$ to the main lobe azimuth width of the antenna, 2) B_ϕ, the ratio of $\Delta\phi$ to the main lobe elevation width, and 3) B_r, the ratio of the depth of the object (in terms of propagation time) to the inverse signal bandwidth:

$$B_\alpha = \frac{\Delta\alpha}{2 \arcsin(\lambda/A_\alpha)}; \quad B_\phi = \frac{\Delta\phi}{2 \arcsin(\lambda/A_\phi)};$$

$$B_r = \left(\frac{2W\Delta r}{c}\right)$$

where λ is the wavelength of the pulse at ω_o ($\lambda = 2\pi c/\omega_o$).

Now consider an object within the volume which is illustrated by an ultrasonic plane wave. Suppose that this object consists only of surfaces located at r_1, $r_1 + \Delta r/M$, $r_1 + 2\Delta r/M$, $\cdots$, $r_2 - \Delta r/M$ where M is an arbitrary integer greater than zero. The excitation $\bar{I}(\alpha, \phi, t)$ can then be expressed as

$$\bar{I}(\alpha, \phi, t) = \sum_{m=0}^{M-1} a(m, \alpha, \phi)\, p(t - m\tau) \tag{17}$$

where[3] $\tau = 2\Delta r/Mc$. We place a constraint on the excitation as follows:

$$\sum_{m=0}^{M-1} \int a^2(m, \alpha, \phi)\, d\alpha\, d\phi \le E. \tag{18}$$

Since the space is limited in extent, $a(m, \alpha, \phi)$ can be expressed as a product of prolate spheroidal wave functions $\psi_k(\alpha)$ and $\psi_l(\phi)$ [9] and the M index-limited discrete prolate spheroidal sequences $v_j(m)$ [10], i.e.,

$$a(m, \alpha, \phi) = \sum_{j,k,l} \alpha_{jkl} v_j(m)\, \psi_k(\alpha)\, \psi_l(\phi). \tag{19}$$

Since the prolate spheroid sequences and wave functions are orthonormal,

$$\sum_{m=0}^{M-1} \int a^2(m, \alpha, \phi)\, d\alpha\, d\phi = \sum_{j,k,l} \alpha_{jkl}^2 \le E. \tag{20}$$

From (16), we conclude that, along the image sphere

$$\begin{aligned} \bar{S}(\theta, \theta', t) &= \boldsymbol{B}_\alpha \boldsymbol{B}_\phi \sum_{m=0}^{M-1} a(m, \alpha, \phi)\, p(t - m\tau) \\ &= \boldsymbol{B}_\alpha \boldsymbol{B}_\phi \sum_{m=1}^{M} \sum_{j,k,l} \alpha_{jkl} v_j(m)\, \psi_k(\alpha) \\ &\quad \cdot \psi_l(\phi)\, p(t - m\tau) \end{aligned} \tag{21}$$

where $\boldsymbol{B}_\alpha$ and $\boldsymbol{B}_\phi$ are the band-limiting operators that are due to the spatial filtering of the lens in the α and ϕ directions, respectively. Since $p(t)$ is band-limited, let $c_j(m)$ be the band-limited version of the index-limited sequence $v_j(m)$. Then, the following orthogonality conditions hold [9]–[11]:

$$\langle c_j, c_k \rangle = \frac{\lambda_j}{2W\tau} \delta_{jk}, \quad j, k = 0, M - 1 \tag{22}$$

$$\langle \boldsymbol{B}_\alpha \psi_j(\alpha), \boldsymbol{B}_\alpha \psi_k(\alpha) \rangle = \lambda_j^{(\alpha)} \delta_{jk}, \tag{23}$$

[3]Note that the factor of 2 is used because we consider both the propagation time to and from the object.

and

$$\langle \boldsymbol{B}_\phi \psi_j(\phi), \boldsymbol{B}_\phi \psi_k(\phi) \rangle = \lambda_j^{(\phi)} \delta_{jk}, \tag{24}$$

where λ_j, $\lambda_j^{(\alpha)}$, $\lambda_j^{(\phi)}$ are the eigenvalues associated with the discrete prolate spheroidal sequence and prolate spheroidal wave functions for α and ϕ, respectively. These eigenvalues are readily determined from M, B_r, B_α, and B_ϕ [9]–[11].

Let

$$c_{jkl}^2 = \frac{\lambda_j \lambda_k^{(\alpha)} \lambda_l^{(\phi)}}{2W\tau} \alpha_{jkl}^2. \tag{25}$$

Then, from (20),

$$\sum_{j,k,l} \alpha_{jkl}^2 = \sum_{j,k,l} \frac{c_{jkl}^2 \cdot 2W\tau}{\lambda_j \lambda_k^{(\alpha)} \lambda_l^{(\phi)}} \leq E. \tag{26}$$

A. Capacity

From (26) we now determine an upper bound on the capacity of the system (number of objects that can be distinguished without error) as a function of B_r, B_α, B_ϕ. Along the image sphere, the distributed receiver is presented with

$$\bar{U}(\theta, \theta', t) = \bar{S}(\theta, \theta', t) + \bar{n}_\omega(\theta, \theta', t) \tag{27}$$

where $\bar{n}_\omega(\theta, \theta', t)$ is additive white Gaussian noise of spectral height $N_o/2$. Since $\bar{S}(\theta, \theta', t)$ has been expressed as the sum of three-dimensional orthogonal modes, the capacity of this three-dimensional system, for an arbitrary partition of the energy E among the modes, is simply

$$C = \sum_{j,k,l} \log_2 \left(1 + E/N_0 \frac{\lambda_j \lambda_k^{(\alpha)} \lambda_l^{(\phi)}}{2W\tau} \beta_{jkl} \right) \tag{28}$$

where β_{jkl} is the fraction of the signal energy apportioned to the jkl mode, subject to the constraint $\sum_{jkl} \beta_{jkl} = 1$. The optimum energy partition that maximizes the capacity can be found by using the water fill analogy [12], i.e.,

$$\beta_{jkl} = \begin{cases} J - \left(\dfrac{\lambda_j \lambda_k^{(\alpha)} \lambda_l^{(\phi)}}{2W\tau} E/N_0 \right)^{-1} \\ \qquad \text{if } \left(\dfrac{\lambda_j \lambda_k^{(\alpha)} \lambda_l^{(\phi)}}{2W\tau} E/N_0 \right)^{-1} < J \\ 0 \quad \text{otherwise} \end{cases} \tag{29}$$

where

$$J = \frac{1}{m} \left(1 + \sum_{j,k,l} \left(\frac{\lambda_j \lambda_k^{(\alpha)} \lambda_l^{(\phi)}}{2W\tau} E/N_0 \right)^{-1} \right) \tag{30}$$

and the sum is over the m terms where

$$\left(\frac{\lambda_j \lambda_k^{(\alpha)} \lambda_l^{(\phi)}}{2W\tau} E/N_0 \right)^{-1} < J.$$

In Fig. 2 we plot the capacity in bits (note that for a capacity of K bits, 2^K objects can be distinguished) versus the received signal energy-to-noise density ratio E/N_o for $B_\alpha = B_\phi = 0.5$ (object space equal to one-half main lobe)

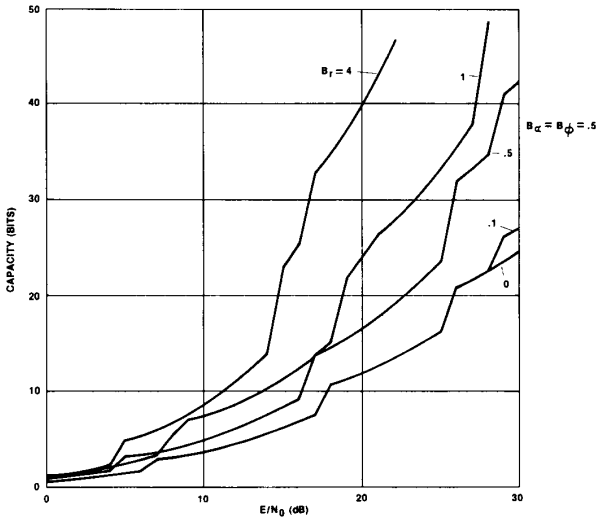

Fig. 2. The capacity versus the received signal energy-to-noise density ratio for $B_\alpha = B_\phi = 0.5$ and several values of B_r.

and several values of B_r. For example, for $B_\alpha = B_\phi = 0.5$, $B_r = 1$, and $E/N_o = 10$ dB, the capacity is 7.5 bits, i.e., up to 180 objects can be distinguished. Thus, our system may be able to distinguish a large number of objects even if their sizes are smaller than the antenna's beamwidth. Also note that even for $B_r = 0$, a large number of objects can be distinguished since the system can distinguish different surfaces in the α, ϕ plane.

Fig. 3 shows the capacity in bits versus E/N_0 for $B_r = 0.5$ and several values of $B_\alpha = B_\phi$. Note again that a large number of objects can be distinguished even if the objects are smaller than the beamwidth, but as the size of the objects decreases the number that can be distinguished goes to 1.

Consider next the capacity for large B_r, B_α, and B_ϕ. Under these conditions, each of the eigenvalues is either very close to unity or very close to zero in value [13]. Then, the capacity can be approximated by

$$C \approx m \log_2 \left(1 + E/N_0 \left(\frac{1}{m} \right) \right) \tag{31}$$

where

$$m = [2B_r + 1] \cdot [2B_\alpha + 1] \cdot [2B_\phi + 1]. \tag{32}$$

For large m,

$$C \approx E/N_0 \cdot \frac{1}{\ln(2)}. \tag{33}$$

Fig. 4 shows the capacity versus E/N_0 for several values of $B_r = B_\alpha = B_\phi$ using (31) and (33). For $B_r = B_\alpha = B_\phi \gg 1$ the capacity rapidly approaches the asymptotic value.

B. Distinguishability under a Fidelity Criterion

The number of objects that can be distinguished with a given error probability can be calculated as follows.

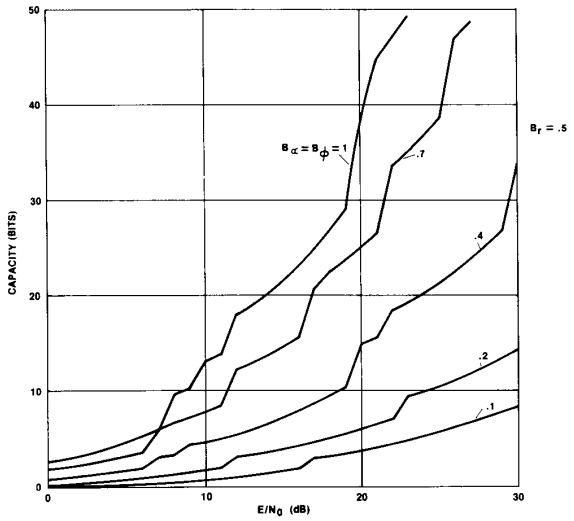

Fig. 3. The capacity versus the received signal energy-to-noise density ratio for $B_r = 0.5$ and several values of $B_\alpha = B_\phi$.

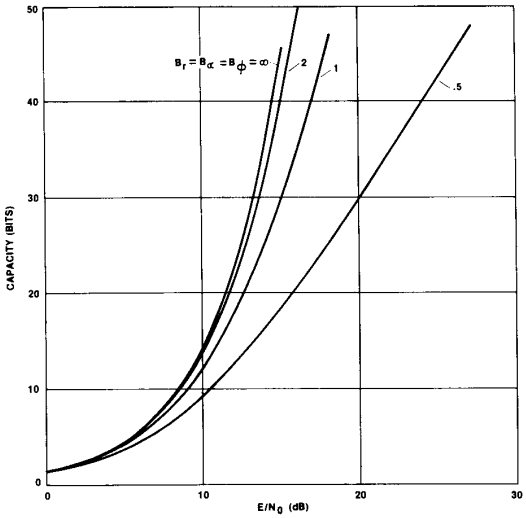

Fig. 4. The capacity versus the received signal energy-to-noise density ratio for several values of $B_r = B_\alpha = B_\phi$ using the formula for large B_r, B_α, and B_ϕ.

Equation (26) is the equation of an infinite dimensional hyperellipsoid with semi-axes of length $\sqrt{\lambda_j \lambda_k^{(\alpha)} \lambda_l^{(\phi)} E/2W\tau}$ or, normalizing all distances by $\sqrt{E}$, $\sqrt{\lambda_j \lambda_k^{(\alpha)} \lambda_l^{(\phi)}/2W\tau}$. For an object to be distinguished with a given error probability, the point in the pattern space corresponding to the object must be separated by a distance d (which depends on the error probability) from all points corresponding to other objects. Thus, an upper bound on the number of objects that can be distinguished subject to a fidelity criterion is the maximum number of nonoverlapping hyperspheres of radius $d/2$ with centers in the hyperellipsoid. This number is upper bounded by the number of hyperspheres of radius $d/2$ that can be placed in an infinite dimensional box with sides of length $2 \cdot \sqrt{\lambda_j \lambda_k^{(\alpha)} \lambda_l^{(\phi)}/2W\tau} + d$, which is upper bounded by the ratio of the content of the box to the content of one hypersphere. Thus, if we consider only the n most significant eigenvalues, the number of objects that can be distinguished is upper bounded by [14]

$$N \le \frac{\prod_{j,k,l} \left[2\sqrt{\dfrac{\lambda_j \lambda_k^{(\alpha)} \lambda_l^{(\phi)}}{2W\tau}} + d \right]}{2\left(\dfrac{d}{2}\right)^n \pi^{n/2} \Big/ \left[n\Gamma(n/2) \right]} = \frac{\prod_{j,k,l} \left[\dfrac{4}{d}\sqrt{\dfrac{\lambda_j \lambda_k^{(\alpha)} \lambda_l^{(\phi)}}{2W\tau}} + 2 \right]}{\dfrac{2\pi^{n/2}}{n\Gamma(n/2)}} \tag{34}$$

where the product is over the n terms.

For given minimum distance d between objects in the pattern space, we now consider the probability of error in detecting an object for a given signal energy-to-noise density ratio E/N_o. We assume that the components of the noise in each dimension are statistically independent, zero-mean, Gaussian random variables. Consistent with an upper bound on N, we determine a lower bound on the probability of error, which for a minimum distance d between objects is given by

$$P_e \ge \frac{1}{2} \operatorname{erfc}\left(\frac{d}{2} \sqrt{E/N_0} \right). \tag{35}$$

Thus, from (34) and (35), we can determine an upper bound on the number of objects that can be distinguished for a given error probability at a given E/N_0. Unfortunately, the tightness of the upper bound decreases dramatically as more eigenvalues are considered, i.e., N increases substantially with n even if the added eigenvalues are negligible. Therefore, for the following results we only consider terms where

$$\frac{\lambda_j \lambda_k^{(\alpha)} \lambda_l^{(\phi)}}{2W\tau} > 10^{-2} d^2. \tag{36}$$

Fig. 5 shows the upper bound on the number of objects that can be distinguished versus $4/d^2$ (for $E/N_0 = 0$ dB) for $B_r = 0.5$ and several values of $B_\alpha = B_\phi$. For fixed P_e, the required E/N_0 is just a constant dB valued added to $4/d^2$. The E/N_0 required for $P_e = 10^{-1}$, 10^{-3}, and 10^{-5} (where the constant values are -0.8, 6.8, and 9.6 dB, respectively) are also shown. For example, for $B_\alpha = B_\phi = 0.3$ and $B_r = 0.5$ up to 1000 objects can be distinguished with a 10^{-3} error probability if E/N_0 is 17 dB. Thus, our results show again that the system may be able to distinguish a large number of objects with good fidelity even if their size is smaller than the antenna's beamwidth. However, since it can be easily shown that $N = 1$ for d

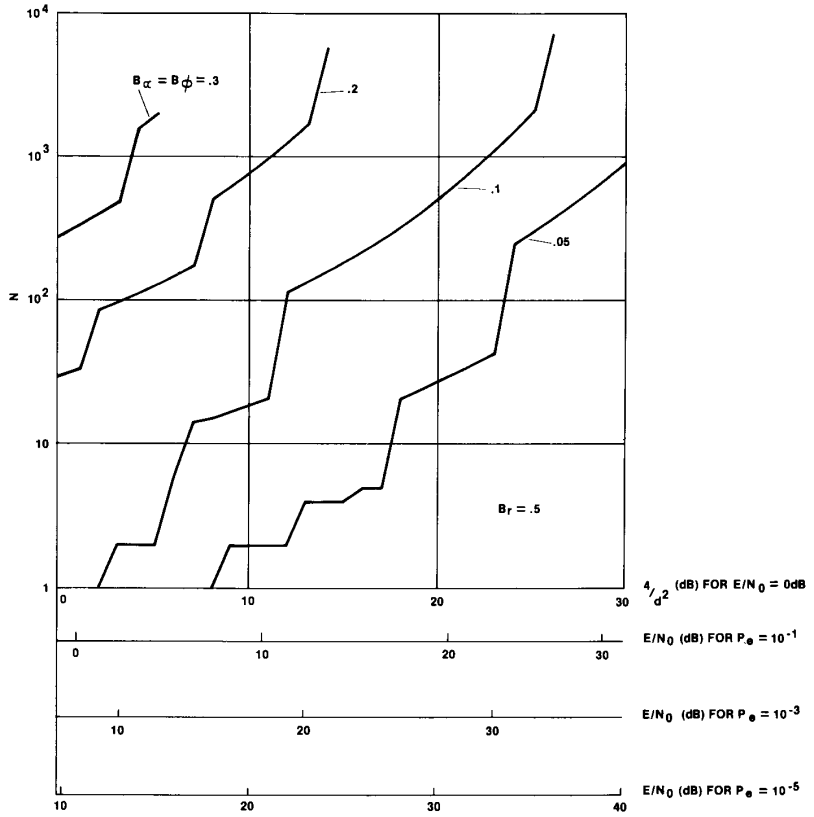

Fig. 5. Upper bound on the number of objects that can be distinguished versus $4/d^2 (E/N_0 = 0$ dB) and $E/N_0 (P_e = 10^{-1}, 10^{-3}, 10^{-5})$ for $B_r = 0.5$ and several values of $B_\alpha = B_\phi$.

$\geq 2 (4/d^2 \leq 0$ dB), Fig. 5 also shows that the bound is very loose, especially for large $B_\alpha = B_\phi$.

Consider next the number of objects that can be distinguished with a given error probability for large B_r, B_α, and B_ϕ. With B_r, B_α, $B_\phi >> 1$, $\lambda_j \lambda_k^{(\alpha)} \lambda_l^{(\phi)} / 2W\tau$ is approximately 1 for $n = (2B_r + 1)(2B_\alpha + 1)(2B_\phi + 1)$ terms and zero for all other terms. Thus, (26) is the equation of an n dimensional hypersphere of radius 1 (normalizing by $\sqrt{E}$), and the number of objects that can be distinguished with a given error probability is the maximum number of nonoverlapping hyperspheres of radius r $(= d/2)$ with centers in the hypersphere of radius 1. Using results appearing in [15], we plot in Fig. 6 the upper bound on the number of objects that can be distinguished versus $4/d^2$ $(E/N_0 = 0$ dB) and E/N_0 $(P_e = 10^{-1}, 10^{-3}, 10^{-5})$ for several values of $B_r = B_\alpha = B_\phi$. For $B_r = B_\alpha = B_\phi = 2$, N is very close to the value for very large B_r, B_α, B_ϕ.

Finally, we note the following limitations to our results on the number of objects that can be distinguished. First, our results are only an upper bound, which may not be very tight, especially for small values of B_r, B_α, B_ϕ. This is seen by noting that the number of objects calculated from the small B_r, B_α, B_ϕ formulas can exceed the bound for large B_r, B_α, B_ϕ even when these parameters are less than 1. Second, our results assume that an object can reflect some of the received energy from internal points. However, most objects act as perfect reflectors to ultrasonic radiation and, therefore, the number of distinguishable objects in the real world may be much less. Third, real objects may not be appropriately spaced in the pattern space, and, therefore, we may be able to distinguish far fewer objects of interest. Furthermore, implementation of techniques to achieve this distinguishability may be difficult because the dimensionality can be large, and features may not be well behaved with respect to object rotation and translation. However, although our results may be much higher than that which can practically be achieved, they do give an upper bound against which practical systems may be compared.

IV. Distinguishability of Common Objects

We now consider the distinguishability of objects with common shapes, in particular, flat plates, edges, and spheres.[4]

In ultrasonics, the attenuation of the signal is a function

[4]As in Section II, to simplify our results the analysis is done in only two dimensions (azimuth *or* elevation and range), since the formulas and results can easily be extended to three dimensions.

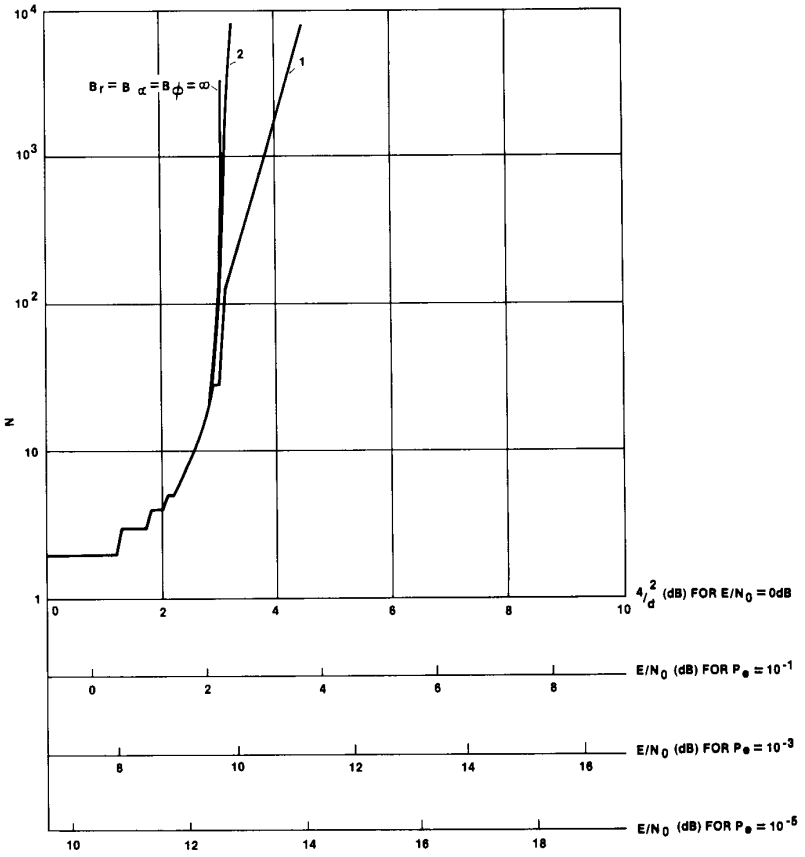

Fig. 6. Upper bound on the number of objects that can be distinguished versus $4/d^2(E/N_0 = 0$ dB) and $E/N_0(P_e = 10^{-1}, 10^{-3}, 10^{-5})$ for several values of $B_r = B_\alpha = B_\phi$.

of both distance and frequency. In this paper, we consider only a narrow-band pulse so that the dispersion of the signal can be neglected. However, the attenuation of the signal with distance at a given frequency can vary significantly with many factors, including temperature and humidity. Thus, the distinguishability of objects greatly depends on whether or not the attenuation versus distance is known. We therefore calculate distinguishability for two cases: 1) where the attenuation versus distance is unknown (and, is therefore not used in calculating distinguishability), and 2) where the attenuation versus distance is known.

Below, we derive from Section II a general formula for the image of arbitrary objects in the time domain, calculate the image for flat plates, edges, and spheres, and analyze the distinguishability for the two cases described above.

A. Time Domain Image

We begin our derivation from (16), and reintroduce the magnitude information dropped after (9), i.e.,

$$\bar{S}(\theta, t) = A \int \left[\int \bar{I}(\alpha, \tau)\, p(t - \tau)\, d\tau \right] \cdot \frac{\sin kA/2(\theta + \alpha)}{kA/2(\theta + \alpha)}\, d\alpha. \tag{37}$$

Let us assume that $\bar{I}(\alpha, \tau)$ can be expressed as $\bar{B}(\alpha, r)$ where r is evaluated at $c(\tau - t_0)/2$ and t_0 is the time when the pulse leaves the plane of the antenna to illuminate the object. That is, $\bar{B}(\alpha, r)$ is the object surface that is not hidden from the view of the antenna in polar (spherical for a three-dimensional object) coordinates, under the assumption that there are no internal reflections on the object. Thus, (37) can be rewritten as

$$\bar{S}(\theta, t) = A \int \left[\int \bar{B}(\alpha, \tau)\big|_{r = c(\tau - t_0)/2}\, p(t - \tau)\, d\tau \right] \cdot \frac{\sin kA/2(\theta + \alpha)}{kA/2(\theta + \alpha)}\, d\alpha. \tag{38}$$

Under the assumption that all surfaces are perfect reflectors, on the object surface (that is not hidden from the view of the antenna) for every α there is only one r, i.e., $r = g(\alpha)$, or

$$\bar{B}(\alpha, r) = \begin{cases} \delta(r - g(\alpha)) & \alpha \in \Omega \\ 0 & \text{elsewhere} \end{cases} \tag{39}$$

where Ω is the region where the surface of the object exists. Noting that

$$\tau = \frac{2g(\alpha)}{c} + t_0 \tag{40}$$

and substituting (39) into (38) we obtain

$$\bar{S}(\theta, t) = A \int_{\Omega} \frac{\sin kA/2(\theta + \alpha)}{kA/2(\theta + \alpha)} \cdot p\left(t - \frac{2g(\alpha)}{c} - t_0\right) d\alpha. \quad (41)$$

Let $g'(\alpha)$ represent distance from a plane directly in front of the object, i.e.,

$$g'(\alpha) = g(\alpha) - R_1 \quad (42)$$

and let

$$t_0 = \frac{-2R_1}{c}. \quad (43)$$

Then, from (41) to (43),

$$\bar{S}(\theta, t) = A \int_{\Omega} \frac{\sin kA/2(\theta + \alpha)}{kA/2(\theta + \alpha)} p\left(t - \frac{2g'(\alpha)}{c}\right) d\alpha. \quad (44)$$

Now consider a pulse with rectangular signal spectrum of bandwidth $4\pi W$ as discussed in Section III. Thus, $p(t)$ is given by

$$p(t) = \frac{\sin 2\pi Wt}{2\pi Wt} \sqrt{2W}\, e^{j\omega_o t} \quad (45)$$

and

$$\bar{S}(\theta, t) = A \int_{\Omega} \frac{\sin kA/2(\theta + \alpha)}{kA/2(\theta + \alpha)} \frac{\sin 2\pi W\left(t - \frac{2g'(\alpha)}{c}\right)}{2\pi W\left(t - \frac{2g'(\alpha)}{c}\right)} \cdot \sqrt{2W} \exp\left[j\omega_o\left(t - \frac{2g'(\alpha)}{c}\right)\right] d\alpha. \quad (46)$$

Finally, to make the results as general as possible, let us normalize all angles, distances, and times by the width of the main lobe and normalize the bandwidth of the pulse by the center frequency, i.e.,

$$z = \frac{\alpha}{\lambda/A}, \quad (47)$$

$$y = \frac{\theta}{\lambda/A}, \quad (48)$$

$$f(z) = \frac{g'(\alpha)}{\lambda R_1/A}, \quad (49)$$

$$t' = \frac{tc}{2\lambda R_1/A}, \quad (50)$$

and

$$\Delta W = \frac{4\pi W}{\omega_o}, \quad (51)$$

with integration over the region Z rather than Ω. Therefore,

$$\bar{S}(y, t') = \lambda \sqrt{2W} \int_Z \frac{\sin \pi(z + y)}{\pi(z + y)} \cdot \frac{\sin\left[2\pi\Delta W R_1/A(t' - f(z))\right]}{2\pi\Delta W R_1/A(t' - f(z))} \cdot \exp\left[j4\pi R_1/A(t' - f(z))\right] dz. \quad (52)$$

Next consider $f(z)$ for a flat plate, edge, and sphere. For each object $f(z)$ can be easily determined. For a flat plate of length D relative to the width of the main lobe and at angle γ to the wavefront (see Fig. 7)

$$f(z) = \begin{cases} (z - z_0)\tan\gamma & 0 \le z - z_0 \le D \\ 0 & \text{elsewhere} \end{cases}. \quad (53)$$

For an edge, with each face of length D relative to the width of the main lobe at angles $\pm\gamma$ to the wavefront (see Fig. 8)

$$f(z) = \begin{cases} (|z - z_0|)\tan\gamma & |z - z_0| \le D \\ 0 & \text{elsewhere} \end{cases}. \quad (54)$$

For a sphere of radius R relative to the width of the main lobe (see Fig. 9)

$$f(z) = \begin{cases} R\left(1 - \sqrt{1 - (z - z_0/R)^2}\right) & |z - z_0| \le R \\ 0 & \text{elsewhere.} \end{cases} \quad (55)$$

To simplify the results, we now assume that z_0 is at the center of the main lobe, i.e., $z_0 = 0$. Thus, the image for flat plates and edges depends only on $\lambda\sqrt{2W}$, R_1/A, ΔW, D, and γ and for spheres depends only on $\lambda\sqrt{2W}$, R_1/A, ΔW, and R. Note that $\lambda\sqrt{2W}$ only affects the magnitude of the image.

Fig. 10 shows the magnitude of the image at $t' = 0$ of a flat plate of various lengths with $\gamma = 0°$, illumination by a pulse. Since the plate is perpendicular to the wavefront, ΔW and R_1/A do not affect the image at $t' = 0$. For $t' \neq 0$, the image has the same shape as at $t' = 0$, but the magnitude varies as $\sin(2\pi\Delta W R_1/At')/(2\pi\Delta W R_1/At')$. For $D \le 1$, the image is very close to a $\sin x/x$ pattern, whose magnitude decreases with D. For $D > 1$, the image approaches a rectangular shape as D increases. Thus, as is well known, the object size must be greater than the beamwidth before the image changes significantly with object size. However, as shown later, even for $D \le 1$ the image changes slightly with D, so that at high enough E/N_0, these objects can be distinguished.

Fig. 11 shows the magnitude of the image at $t' = 0$ of a flat plate of the same width as the main lobe at various angles γ relative to the wavefront. Results are shown for $R_1/A = 10$ and $\Delta W = 0.1$. Note that the peak image level is down 10 dB at $\gamma = 5°$. For small γ, $\tan\gamma \approx \gamma$, and, therefore, from (52) results depend primarily on the product $\gamma R_1/A$. Thus, the peak image level is also down 10 dB for $R_1/A = 20$ at $\gamma = 2.5°$, for $R_1/A = 5$ at $\gamma =$

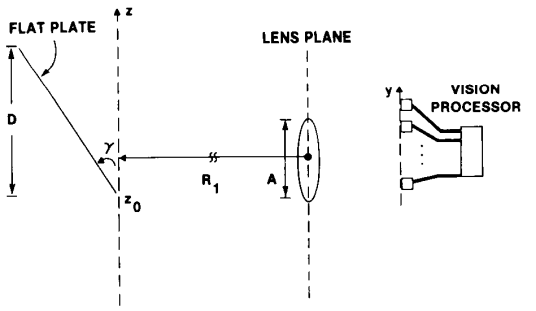

Fig. 7. Flat plate at angle γ relative to the wavefront.

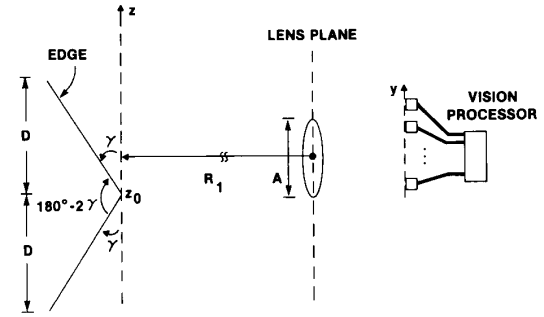

Fig. 8. Edge of angle $180° - 2\gamma$.

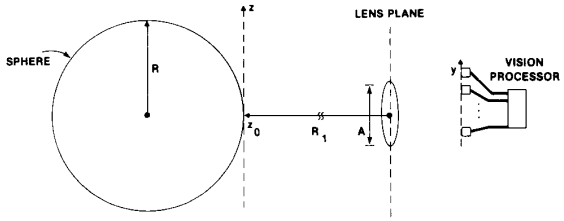

Fig. 9. Sphere of radius R.

10°, etc. Thus, unless R_1/A is very small, the magnitude of the return from most surfaces of objects will be very low.

Fig. 12 shows the magnitude of the image versus time of a flat plate of the same width as the main lobe at $\gamma = 5°$. Note that the image is basically a $|\sin x/x|$ in space and time, i.e., except for an overall magnitude reduction the image is about the same as for a plate at $\gamma = 0°$. Thus, the depth resolving capability of the ultrasonic system does not significantly increase the distinguishability of flat plates at various angles. Note that we can increase the depth of the plate by increasing γ or R_1/A (for the same D), but, as noted above, this reduces the magnitude of the image.

Fig. 13 shows the magnitude of the image at $t' = 0$ of an edge with each face at angle γ to the wavefront and of the same width as the main lobe. Results are shown for $R_1/A = 10$ and $\Delta W = 0.1$. The image peaks at $y = 0$ and is the sum of the images of the two flat plates that make up the edge.

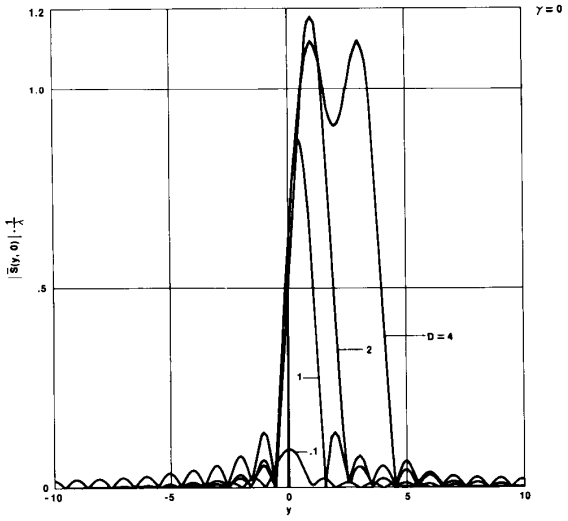

Fig. 10. Magnitude of the image at $t' = 0$ of a flat plate of various lengths with $\gamma = 0°$ for illumination by a pulse.

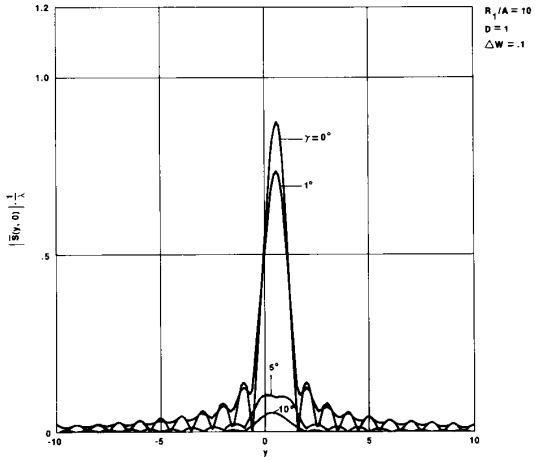

Fig. 11. Magnitude of the image at $t' = 0$ of a flat plate for various angles γ to the wavefront.

Fig. 14 shows the magnitude of the image at $t' = 0$ of a sphere of various radii illuminated by a pulse with $\Delta W = 0.1$ and $R_1/A = 10$. For a sphere, the image mainly consists only of the portion of the surface where the angle of the surface to the wavefront is small (as expected from the results for flat plates). Thus, the sphere must be much larger than the main lobe before the image at $t' = 0$ changes significantly with the sphere size. As seen in Fig. 14, even for $R = 5$, the shape of the image is about the same as with much smaller values of R. Furthermore, for larger values of R_1/A, even less of the surface can be seen. Thus, as before, R_1/A must be small if we are to see and distinguish spheres.

B. Distinguishability

We now consider the distinguishability of common objects, in particular spheres. Spheres represent a worst case

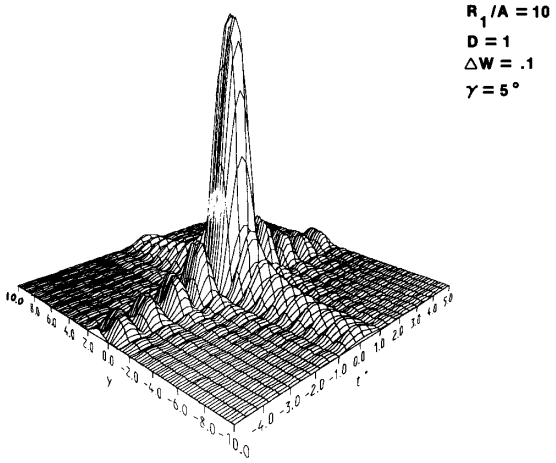

Fig. 12. Magnitude of the image versus normalized distance y and time t' of a flat plate.

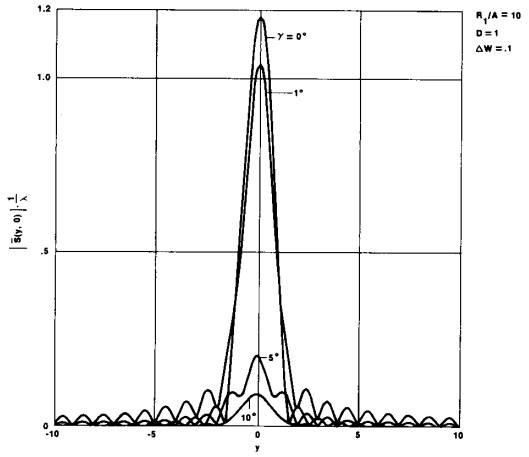

Fig. 13. Magnitude of the image at $t' = 0$ of an edge of angle $180° - 2\gamma$.

since, from Section IV-A, the shape of the magnitude of the image changes very little with sphere radius. However, time-of-flight information can also be utilized to improve the distinguishability of spheres. Note that we can distinguish spheres from flat plates and edges and distinguish flat plates and edges of various sizes with much greater reliability.

We determine the distinguishability of two objects by calculating the metric distance between the image of these objects when they are illuminated by a pulse with spectrum $P(\omega)$. Thus, the distance is given by

$$d = \left[\int\int \left| \frac{\bar{S}_1(\theta, t)}{c_1} - \frac{\bar{S}_2(\theta, t)}{c_2} \right|^2 d\theta \, dt \right]^{1/2} \tag{56}$$

where $\bar{S}_1(\theta, t)$ and $\bar{S}_2(\theta, t)$ are the images of object 1 and 2, respectively, and c_1 and c_2 depend on which of the two cases (as discussed previously) are considered. For the case 1 where the attenuation versus distance is unknown,

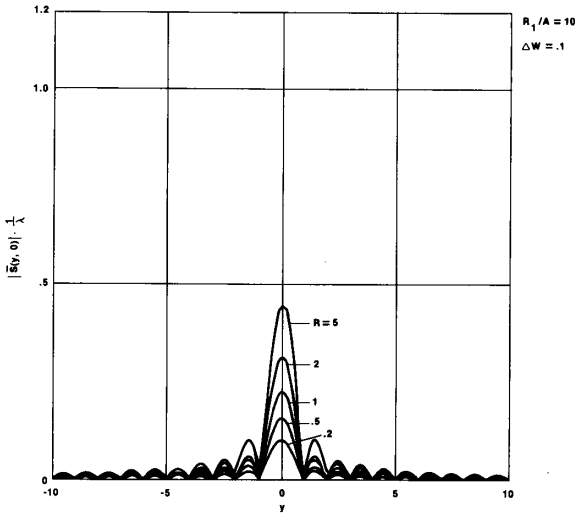

Fig. 14. Magnitude of the image at $t' = 0$ of a sphere of various radii.

c_1 and c_2 are given by

$$c_1 = \begin{cases} 1 & a_1 \geq a_2 \\ \dfrac{a_1}{a_2} & a_1 < a_2 \end{cases} \tag{57}$$

and

$$c_2 = \begin{cases} 1 & a_2 \geq a_1 \\ \dfrac{a_2}{a_1} & a_1 < a_2 \end{cases} \tag{58}$$

where

$$a_{1,2} = \left[\int\int \left| \bar{S}_{1,2}(\theta, t) \right|^2 d\theta \, dt \right]^{1/2}. \tag{59}$$

For case 2 where both the attenuation versus distance and frequency are known, we set

$$c_{1,2} = 1. \tag{60}$$

Thus, using the normalizing parameters of Section IV-A, the distance can be expressed as

$$d = \left[\frac{\lambda}{A} \frac{1}{2W} \int\int \left| \frac{\bar{S}_1(y, t')}{c_1} - \frac{\bar{S}_2(y, t')}{c_2} \right|^2 \cdot dy \frac{dt'}{\left(\dfrac{1}{2\Delta W R_1/A} \right)} \right]^{1/2}. \tag{61}$$

Since $\bar{S}_{1,2}(y, t')$ [(52)] have a constant factor of $\lambda\sqrt{2W}$, from (61) we can obtain results for the distance as a function of ΔW, R_1/A, D, and γ for flat plates and edges, and ΔW, R_1/A, and R for spheres, times a constant factor of λ^3/A. (Note that $a_{1,2}$ (and $c_{1,2}$) can also be calculated from the normalized image without changing the distance results.)

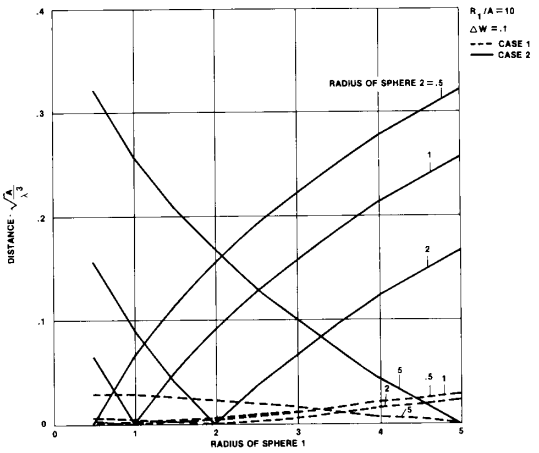

Fig. 15. Metric distance between the image of two spheres when illuminated by a pulse.

Fig. 15 shows the metric distance between two spheres of various sizes when the spheres are illuminated by a pulse with bandwidth $\Delta W = 0.1$. Results are shown for cases 1 and 2. For case 1 the distance is very small, as expected from Fig. 14 since the shape of the image is basically a $|\sin x/x|$ for spheres of radius up to 5. Thus, for this case, E/N_0 must be very large to distinguish one sphere from another. For case 2 where the magnitude of the image is used, the distance is at least ten times larger than for case 1. Thus, the E/N_0 required to distinguish spheres with a given error probability is about 20 dB lower than for case 1.

V. Conclusions

We have proposed the use of ultrasonic pulsing combined with parallel signal processing to facilitate the process of machine vision, and have explored the fundamental resolution limitations presented by such a system. The use of information received along the aperture of a planar antenna plus time-of-flight data permits an object to be cataloged in accordance with its three-dimensional acoustic signature. As with any imaging system, the ability to distinguish among signatures of different objects is dependent on the relationship between the extent of the objects (in degrees) and the size of the receiving aperture (in wavelengths). With ultrasonics (as opposed to optics), this becomes an important consideration since the size of the receiving aperture (again, in wavelengths) is relatively small. However, our results indicate that, even for objects constrained in size to be smaller than a beamwidth, the number of such objects that may be distinguished is quite large; the nonzero radial range extent of an object helps in this regard since time-of-flight information is available. Thus, techniques such as we describe may be an important supplement to or substitute for conventional vision systems. Among the advantages offered are reduced information processing (faster speed), less clutter (all three dimensions are used), and total avoidance of the need to reconstruct accurate visual images (which may include much unwanted information).

However, ultrasonic reflections tend to be specular, and only a small portion of an object may thereby be visible to such a system. Furthermore, the medium (air) tends to be both lossy and dispersive at ultrasonic frequencies. Finally, to fully exploit the potential offered by such a system, more work needs to be directed along the following fronts.

1) Useful signal processing algorithms to rapidly extract relevant information,

2) greater understanding of how objects may be classified with regard to rotations which may bring the dark side of an object into view, and

3) experimental verification and feasibility demonstration of the concepts involved.

Acknowledgment

We gratefully acknowledge useful discussions with C. Rose and R. Mammone and the programming assistance of J. MacLellan.

References

[1] D. Nitzan, "Development of intelligent robots: Achievements and issues," *IEEE J. Robot. Automat.*, vol. RA-1, Mar. 1985.

[2] M. K. Brown, "Locating object surfaces with an ultrasonic range sensor," in *Proc. 1985 IEEE Int. Conf. Robot. Automat.*

[3] J. S. Schoenwald and J. F. Martin, "Acoustic scanning for robotic range sensing and object pattern recognition," in *Proc. 1982 IEEE Ultrason. Symp.*

[4] R. C. Bryant and R. F. Bogner, "Ultrasonic surface imaging in adverse environments," *IEEE Trans. Sonics Ultrason.*, vol. SU-31, pp. 373-390, July 1984.

[5] H. P. Moravec and A. Elfes, "High resolution maps from wide angle sonar," in *Proc. 1985 IEEE Int. Conf. Robot. Automat.*

[6] J. M. Richardson, K. A. Marsh, J. S. Schoenwald, and J. F. Martin, "Acoustic imaging of objects in air using a small set of transducers," in *Proc. 1984 IEEE Ultrason. Symp.*

[7] K. A. Marsh, J. M. Richardson, J. F. Martin, and J. S. Schoenwald, "Acoustic imaging in robotics using a small set of transducers," in *Proc. 4th Int. Conf. Robot Vis. Sensory Cont.*, 1984.

[8] S. Buckley, "Acoustic inspection of parts using microprocessors," *Proc. Autofact West, CAD/CAM VIII*, vol. 1, pp. 571-588, Nov. 17-20, 1980.

[9] H. J. Landau and H. O. Pollack, "Prolate spheriodal wave functions, Fourier analysis, and uncertainty-III," *Bell Syst. Tech. J*, vol. 41, pp. 1295-1336, July 1962.

[10] D. Slepian, "Prolate spheriodal wave functions, Fourier analysis, and uncertainty-V: The discrete case," *Bell Syst. Tech. J.*, vol. 57, pp. 1371-1430, May-June 1978.

[11] A. D. Wyner, "Signal design for PAM data transmission to minimize excess bandwidth," *Bell Syst. Tech. J.*, vol. 57, pp. 3277-3307, Nov. 1978.

[12] R. G. Gallager, *Information Theory and Reliable Communication*. New York: Wiley, 1968, p. 344.

[13] H. L. Van Trees, *Detection, Estimation, and Modulation Theory, Part I*. New York: Wiley 1968, p. 193.

[14] M. G. Kendall, *A Course in the Geometry of n Dimensions*. New York: Hafner, 1961.

[15] N. H. Blachman, "The closest packing of equal spheres in a larger sphere," *Amer. Math. Month.*, vol. 70, pp. 526-529, 1963.

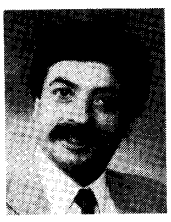

Anthony S. Acampora (S'68-M'75-SM'86-F'88) was born in Brooklyn, NY, on December 20, 1946. He received the B.S.E.E., M.S.E.E., and Ph.D. degrees from the Polytechnic Institute of Brooklyn in 1968, 1970, and 1973, respectively.

From 1968 through 1981, he was a member of technical staff at Bell Laboratories initially working in the fields of high power microwave transmitters and radar system studies and signal processing. From 1974 to 1981, he was involved in